Fluoride removal performance and mechanism of superparamagnetic Fe$_3$O$_4$ nanoparticles

Kaisheng Zhang[a,*,†], Baisheng Zhu[a,†], Wu Yang[b,†], Yong Jia[a], Peijuan Jiang[c], Qiang Zhang[c], Lingtao Kong[a,*], Jinhuai Liu[a]

[a]*Environmental Materials and Pollution Control Laboratory, Institute of Solid State Physics, HFIPS, Chinese Academy of Sciences, Hefei 230031, China, Tel. +86-551-65591142; Fax: +86-551-65592420; emails: kszhang@iim.ac.cn (K.S. Zhang), ltkong@iim.ac.cn (L.T. Kong), 921503544@qq.com (B.S. Zhu), yjiaahedu@163.com (Y. Jia), jhliu@iim.ac.cn (J.H. Liu)*
[b]*Institutes of Physical Science and Information Technology, Anhui University, Hefei 230601, China, email: 379494361@qq.com (W. Yang)*
[c]*Anhui Environmental Science and Technology Group Co., Ltd., China, emails: jiangpj@ahest.cn (P.J. Jiang), zq1981449@sohu.com (Q. Zhang)*

ABSTRACT

Fluoride contamination in drinking water is one of the major problems worldwide imposing a serious threat to human health. For fluoride removal, the superparamagnetic Fe$_3$O$_4$ nanoparticles (Fe$_3$O$_4$ NPs) were successfully synthesized in a non-aqueous medium through a simple and facile hydrothermal reduction route. These nanoparticles had a mesoporous structure with a specific surface area of 70.14 m^2 g^{-1}. Fluoride adsorption behavior was investigated and the optimization of several experimental parameters was explored. The adsorption properties of the sample were excellent. The adsorption capacity could reach up to 70.64 mg g^{-1} at 25°C when the initial fluoride concentration was 200 mg L^{-1}. Kinetic data were consistent with the pseudo-second-order model and also indicated the adsorption process was limited by the pore diffusion. The adsorption isotherms were found fitting well with the Freundlich model. The presence of bicarbonate, carbonate, and phosphate adversely affected the adsorption of fluoride. The revelation of the adsorption mechanism was based on Fourier transform infrared spectroscopy, X-ray photoelectron spectroscopy analysis, and zeta potential study. The results showed the surface hydroxyl groups and sulfate anions played important roles in the fluoride removal. In the magnetic hysteresis curves, the Fe$_3$O$_4$ nanoparticles exhibited a superparamagnetic characteristic with a saturation magnetization of 29.86 emu g^{-1}, which was beneficial for magnetic separation.

Keywords: Fluoride removal; Adsorption; Fe$_3$O$_4$ nanoparticles; Ion-exchange; Hydroxyl groups

1. Introduction

Classified as one of the abundant trace elements in the Earth's crust with an average concentration of 625 mg kg^{-1}, fluoride is primarily enriched in such minerals as fluorite, cryolite, fluorapatite, topaz, biotites, villiaumite, and certain clays [1]. Natural processes, combined with biological activity and anthropogenic activity allow the release of fluoride into water resources, causing many districts worldwide with more than 250 million people still suffering from fluoride contaminated water [2,3]. Due to its high toxicity, the long-term and excessive ingestion of fluoride have great adverse effects on human health, which should be responsible for various diseases [4,5]. The epidemiological studies reveal that continuous consumption of drinking water with heightened fluoride concentrations can lead to the incidence of dental caries, brain damage, thyroid disorder, and infertility [6]. Thus, the World Health Organization (WHO) has specified the guideline value

* Corresponding author.

† These authors contributed equally to this work.

of fluoride content of drinking water as 1.5 mg L^{-1} [7,8]. Undoubtedly, it is urgently needed to develop economical, reliable, and eco-friendly techniques for water purification. Among the various technologies available for fluoride removal, the adsorption process is generally accepted as the cheapest and most effective method compared with ion exchange, membrane separation, and others [9]. A significant variety of adsorbents have been investigated to remove fluoride and the adsorbents include clays, minerals, activated carbon and nanotubes, rare oxides, and polymeric materials [10]. It is reported that the existence of high-valency metal ions like iron (III), manganese (II, IV), lanthanum (III), aluminum (III), zirconium (IV), or titanium (IV) can significantly increase fluoride adsorption capacity [11,12]. However, when it comes to chemical stability, low cost, large storage, high affinity, and environmental friendliness, iron-based materials seem to be the most promising adsorbents. Indeed, these adsorbents have attracted increasing attention and have been applied successfully for fluoride remediation. The group of Kumar evaluated the feasibility of granular ferric hydroxide [13]. Mohapatra and colleagues developed magnesium-doped nanoferrihydrite for defluoridation [14]. Mohapatra and coworkers investigated the fluoride adsorption behavior of Hexadecyl trimethyl ammonium Bromide (CTAB) mediated Mg-doped nano Fe$_2$O$_3$ [15]. Poursaberi et al. reported the synthesis of zirconium (IV)-metalloporphyrin grafted Fe$_3$O$_4$ nanoparticles [16]. Bhaumik's team published a study of polypyrrole/Fe$_3$O$_4$ magnetic nanocomposite to remove fluoride [17]. As a common iron oxide, magnetite (Fe$_3$O$_4$) nanoparticles are popular in adsorbents mainly because of their unique and tunable magnetic properties which contribute significantly to solid–liquid phase separation. Here, it should be pointed out that magnetic separation appears to be a very outstanding method for separation, considering its prominent advantages of effective control, high speed, accuracy, and simplicity over centrifugation or filtration [18].

However, it was also well-known that the properties of Fe$_3$O$_4$ based materials strongly depended on their structure and morphology [19]. The different selections of iron sources and chemistry-based synthetic methods lead to a wide variety of morphologies [20,21]. Though Fe$_3$O$_4$ just acts as a carrier material at the most times applied for magnetic separation in fluoride removal, it is still challenging to develop a simple, low-cost, and environmentally friendly green route for synthesizing Fe$_3$O$_4$ nanoparticles for defluoridation [16,22,23]. To overcome these limitations and cater for better industrial application, our interest is to develop a Fe$_3$O$_4$ adsorbent with excellent fluoride removal properties. Herein, drawing inspiration from the previous work of natroalunite microtubes [24], we successfully synthesized superparamagnetic Fe$_3$O$_4$ nanoparticles in a non-aqueous medium via a simple and facile hydrothermal reduction route using a single iron precursor, Fe$_2$(SO$_4$)$_3$. Furthermore, the fluoride adsorption performances were investigated. A series of adsorption experiments including adsorption kinetics, adsorption isotherm, and impact of pH value and co-existing anions, were conducted to examine the adsorption behavior. The results showed that the adsorption performances of superparamagnetic Fe$_3$O$_4$ nanoparticles toward fluoride were incredibly wonderful. In addition,

X-ray photoelectron spectroscopy (XPS), Fourier transform infrared spectroscopy (FT-IR) and zeta potential study revealed the key roles of the surface hydroxyl groups and sulfate anions in the adsorption process.

2. Experimental section

2.1. Materials and synthesis

All reagents involved in the study were analytical grade, purchased from Shanghai Chemical Reagents Company and used without further purification. The Fe$_3$O$_4$ nanoparticles were prepared in a facile hydrothermal reduction route. 0.3 g of poly(vinylpyrrolidone) (PVP, K30) was dissolved into 100 mL ethylene glycol (EG) with stirring. After the solution turning clear, 3.0 g of iron(III) sulfate was added into the above solution. When iron(III) sulfate was dissolved completely, 3.69 g of sodium acetate anhydrous was put into the mixture. The solution was under vigorous stirring for another 6 h, then sealed in a Teflon-lined stainless steel autoclave and heated at 180°C for 12 h before cooled naturally to room temperature. The residues were centrifuged and thoroughly washed with distilled water and absolute ethanol, and finally dried in a vacuum to form a black powder.

2.2. Characterization

Powder X-ray diffraction (XRD) analyses were carried out to identify the mineralogical phases and crystallinity of the samples. The Raman spectrum was obtained with a Raman microscopy spectrometer (Lab RAM HR, HORIBA Scientific, Japan). Transmission electron microscope (TEM) was operated to observe the particle size and morphology. X-ray photoelectron spectroscopy (XPS) studies were undertaken for quantitative estimation of chemical elements of the adsorbents before and after adsorption. Fourier transform infrared spectra (FT-IR) were collected on a NEXUS-870 spectrometer. The specific surface area was determined by the low-temperature N$_2$ adsorption-desorption technique using a micrometrics surface area analyzer with a degassing temperature of 80°C. The magnetic properties were measured using a Quantum Design MPMS XL-5 superconducting quantum interference device.

2.3. Adsorption experiments

A fluoride ion stock solution (200 mg L^{-1}) of sodium fluoride was prepared in deionized water and stored in a polyethylene bottle. The test solutions were made by subsequent dilution of the fluoride solution to a certain concentration. A series of experiments on fluoride uptake was performed, involving adsorption isotherms, adsorption kinetics, and the effects of other parameters. The adsorption isotherm experiments were carried out in 15 mL conical-bottom polypropylene tubes at pH 7.0. The initial fluoride concentration was varied from 5 to 200 mg L^{-1}. In each of 15 mL polyethylene tubes, 10 mg of adsorbent was mixed with 10 mL of fluoride solutions that had different initial concentrations. The mixtures were shaken on an orbit shaker at 150 rpm for 24 h at 25°C, 35°C, and 45°C, respectively. At the end of the experiment, the

samples were filtered by a membrane filter with 0.22 µm pore size. The fluoride concentration of the filtrate was determined by a fluoride meter.

An adsorption kinetics experiment was conducted with an initial fluoride concentration of 2.5 mg L^{-1}. Herein, 300 mg of adsorbent and 300 mL of predetermined fluoride solution were contained in a 500 mL polypropylene bottle and stirred at 25°C with pH controlled at 7.0. At a fixed preselected interval time from 0.1 to 360 min, about 4 mL of suspension was withdrawn and filtered for analysis. To determine the chemical condition at which fluoride ions are effectively adsorbed, optimization of the main factors was explored, namely adsorbent dosage, pH value, and coexisting anions. The impact of the adsorbent dosage in fluoride removal was tested by varying the amount of the adsorbent from 5 to 200 mg while other parameters have remained the same. To evaluate the influence of pH value on fluoride adsorption, the initial solution pH was adjusted from 3 to 11 with dilute HCl or NaOH solution. And then, the fluoride solutions with different concentrations were mixed with 100 mg adsorbent, respectively, and shaken continuously in an incubator for 24 h at 25°C. Afterward, approximately 4 mL of suspension was sampled for analysis to obtain the residual fluoride concentration.

For the investigation of the competitive effects of various coexisting anions on fluoride removal, competing anions solutions (chloride, nitrate, sulfate, bicarbonate, carbonate, and phosphate) were prepared with concentrations ranging from 0 to 200 mg L^{-1}. As the experiments performed, 100 mg adsorbent was contacted with solutions containing both fluoride and coexisting anions for 24 h. Then, the samples were extracted and centrifuged to collect the supernatant liquid for analysis.

Each adsorption experiment was performed in triplicate to reap reproducible results with an error of less than 5%. The residual fluoride concentration of the clear liquid samples obtained during the above tests was measured with a fluoride ion-selective electrode (PF-202-CF) by utilizing a total ionic strength adjustment buffer (TISAB) solution to eliminate the interference of complexing ions. The amount of fluoride adsorbed (q_e in mg g^{-1}) was determined by Eq. (1) and the fluoride removal efficiency (R_F) was calculated according to Eq. (2) [25,26]:

$$q_e = \left(C_0 - C_e \right) \frac{V}{m} \tag{1}$$

$$R_F = \frac{\left(C_0 - C_e \right)}{C_0} \times 100\% \tag{2}$$

where V is the total solution volume (mL), m is the mass of adsorbent (mg); C_0 and C_e are the fluoride concentration in the liquid phase at initial and equilibrium (mg L^{-1}), respectively.

3. Results and discussion

3.1. Characterization

An X-ray diffraction pattern of the obtained product can seen in Fig. 1a. There were six diffraction peaks observed, which were corresponding to the (220), (311), (400), (422), (511), and (440) planes of Fe$_3$O$_4$ (JDPCS card number 19-0629). No characteristic peaks from impurities were detected. However, it is well known that the XRD pattern of Fe$_3$O$_4$ was almost the same as that of γ-Fe$_2$O$_3$. Thus, the structure of the obtained products cannot be discriminated by XRD alone. To further confirm the structure of the products, the obtained products were characterized by Raman microscopy, and the results are shown in Fig. 1b. The Raman peak around 670 cm^{-1} was observed that was the typical characteristic of Fe$_3$O$_4$. While for γ-Fe$_2$O$_3$, three strong peaks are generally found at 352, 500 and 695 cm^{-1}, respectively [27]. To further confirm the XRD results, the oxidation states and composition of the products were examined by XPS. The XPS survey spectrum of the sample displayed in Fig. 1c showed the predominant signals of carbon, oxygen, and iron. The Fe 2p spectrum was seen in Fig. 1d, which revealed the presence of Fe^{3+} and Fe^{2+}. The peak around 710.4 eV was assigned to a Fe^{III}3/2 configuration. The other spin-orbit component, Fe 2p$_{1/2}$, appearing at 724.4 eV, was corresponding to Fe(III) and Fe(II) states. Another two weak peaks at 719.3 eV and 732.6 eV were the Fe^{2+} shaking up satellite peaks [28,29]. So, the results confirmed that the obtained products were Fe$_3$O$_4$.

The as-synthesized Fe$_3$O$_4$ was further characterized by TEM, and the results are shown in Fig. 2. In Fig. 2a, it was noted that the product has consisted of a large number of nanoparticles and the particle size was mostly below 100 nm with an average value in the range 70~80 nm. To be precise, the nanoparticles were sphere-like rather than spherical as illustrated in Fig. 2b. Interestingly, it was also found these nanoparticles were the agglomerates of smaller particles, suggesting that the sample might have a mesoporous structure.

As an important factor affecting the adsorption behavior, the BET surface area of the Fe$_3$O$_4$ NPs was measured before the adsorption experiments, the results are revealed in Fig. 3. According to the IUPAC classification, the N$_2$ adsorption-desorption isotherm in Fig. 3a was a typical type IV isotherm with a H1 hysteresis loop, confirming the mesoporous structure of Fe$_3$O$_4$ NPs. The BET surface area was 70.14 m^2 g^{-1}, which was larger than those of some other adsorbents [30,31]. The corresponding BJH pore size distribution curve is presented in Fig. 3b. It was worth noticed that two different pore sizes emerged in the graph. One with an average pore diameter at 3.6 nm whose pore volume was 0.211 cm^3 g^{-1}, and the other at 34 nm [32]. The former was from the internal structure of Fe$_3$O$_4$ NPs and the latter was caused by the aggregation of Fe$_3$O$_4$ NPs.

The magnetic properties of the Fe$_3$O$_4$ nanoparticles were investigated. Fig. 4 shows the magnetic hysteresis curves measured at 300 K, with the field sweeping from –60,000 to 60,000 Oe. With a saturation magnetization of 29.86 emu g^{-1}, the Fe$_3$O$_4$ nanoparticles exhibited a superparamagnetic characteristic [33,34]. It was reported that there were many factors such as particle size, crystallinity, surface disorder, and surface ligands, which could affect the magnetic properties of nanoparticles. The Fe$_3$O$_4$ nanoparticles in this work embraced a high saturation magnetization. The magnetic property made the adsorbent easy to retrieve from the solution using an external magnetic field (Fig. S1).
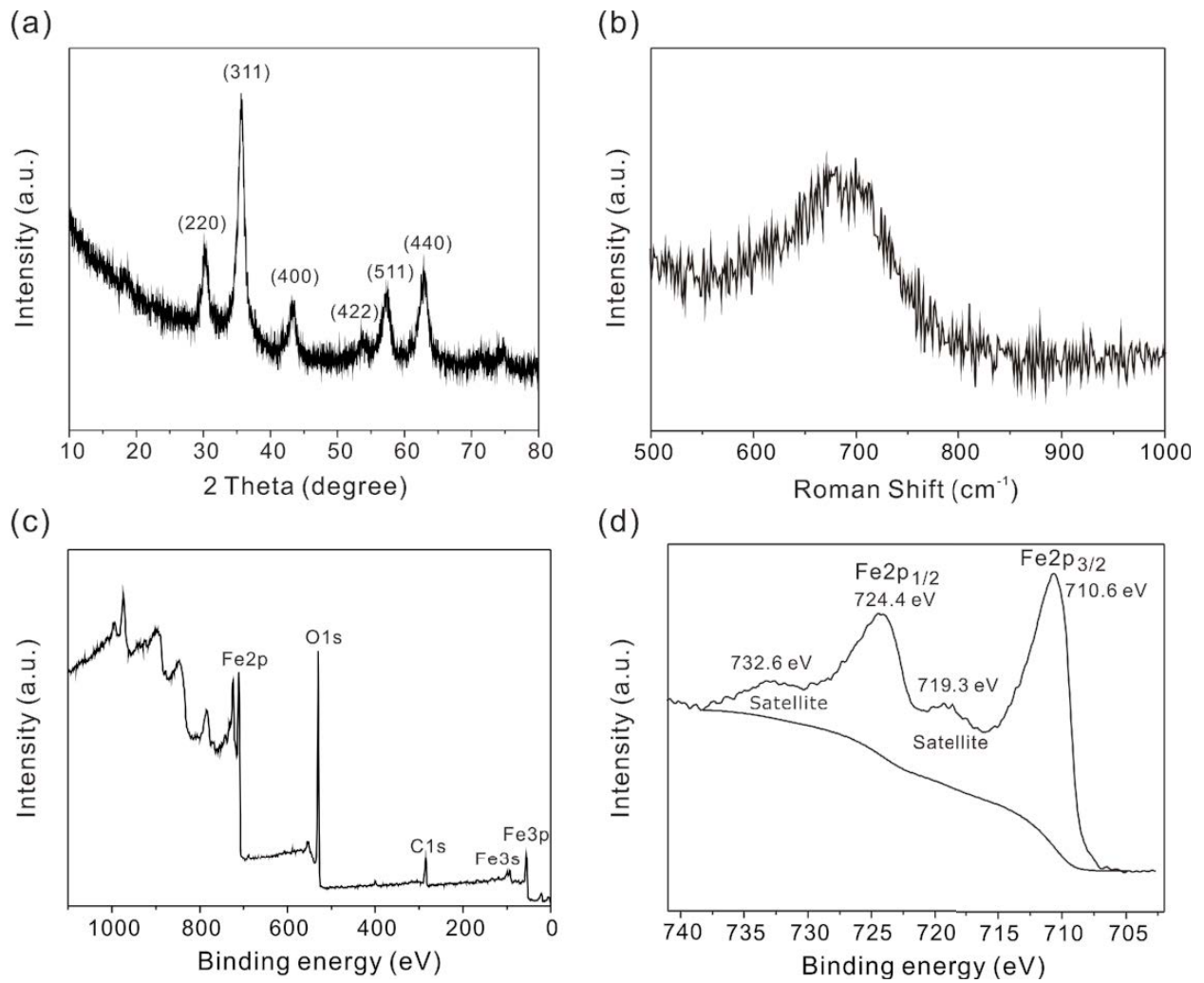
Fig. 1. XRD pattern (a), Raman spectroscopy (b) and XPS survey(c), Fe 2p spectra (d) of the obtained product.
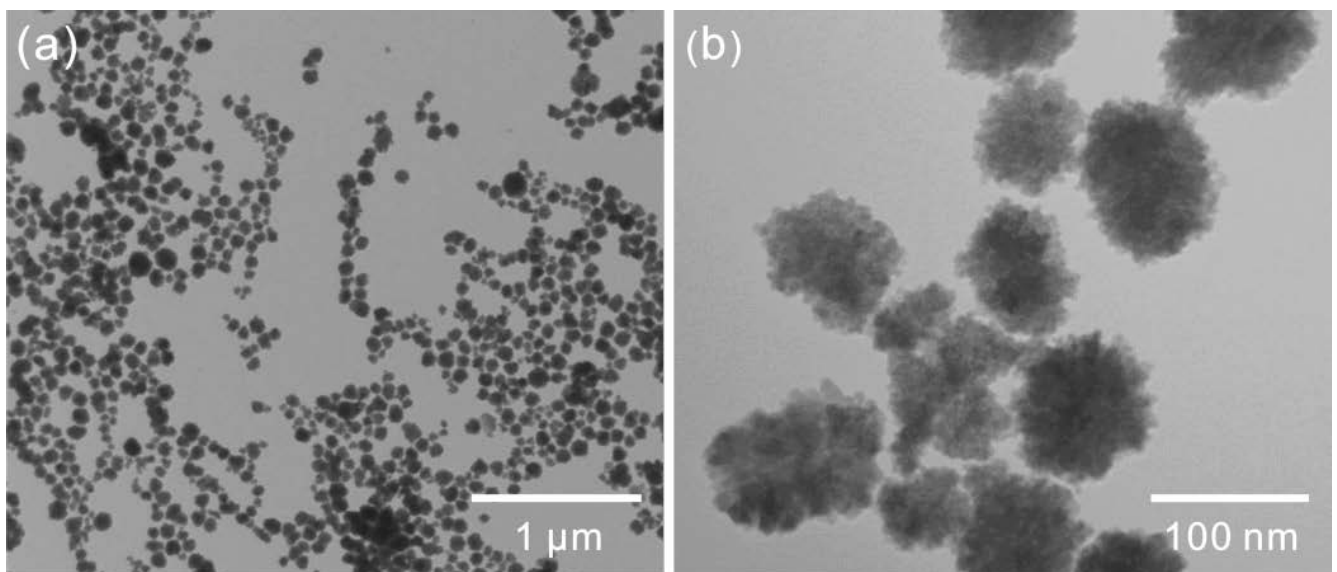

Fig. 2. Low-magnification (a) and high-magnification (b) TEM images of Fe_3O_4 nanoparticles.
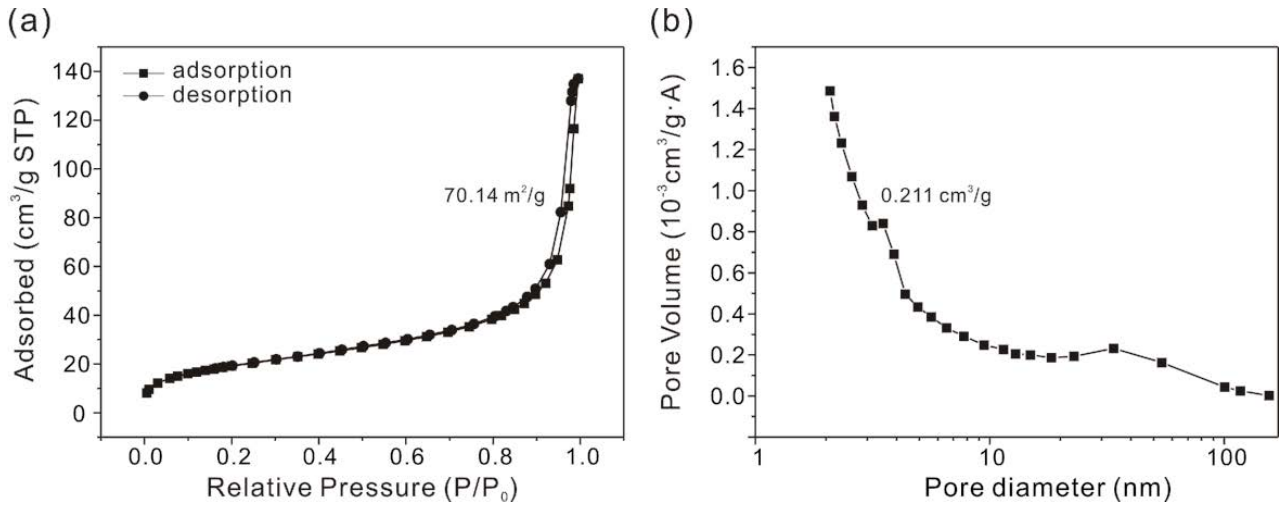
Fig. 3. Nitrogen adsorption–desorption isotherm (a), and the pore-size distribution curve (b) of Fe_3O_4 nanoparticles.
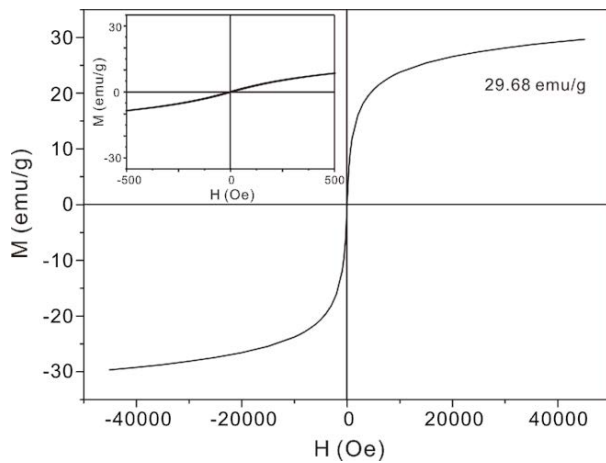

Fig. 4. Magnetization curves of Fe_3O_4 nanoparticles.

This feature further pushed the application of Fe_3O_4 NPs adsorbent under the spotlight for fluoride removal.

3.2. Adsorption studies

3.2.1. Adsorption kinetic studies

Adsorption kinetics is one of the most important characters which represent adsorption efficiency. The fluoride adsorption performance of the obtained Fe_3O_4 NPs was investigated and its results are displayed in Fig. 5. Obviously, adsorption was rapidly improved at the initial stages within 60 min. To further research the process of adsorption with time, these experimental data were dealt with the pseudo-first-order and pseudo-second-order kinetic models, respectively, and shown in Table 1. It could be observed the coefficient ($R^2 > 0.999$) of the pseudo-second-order was much higher than that of
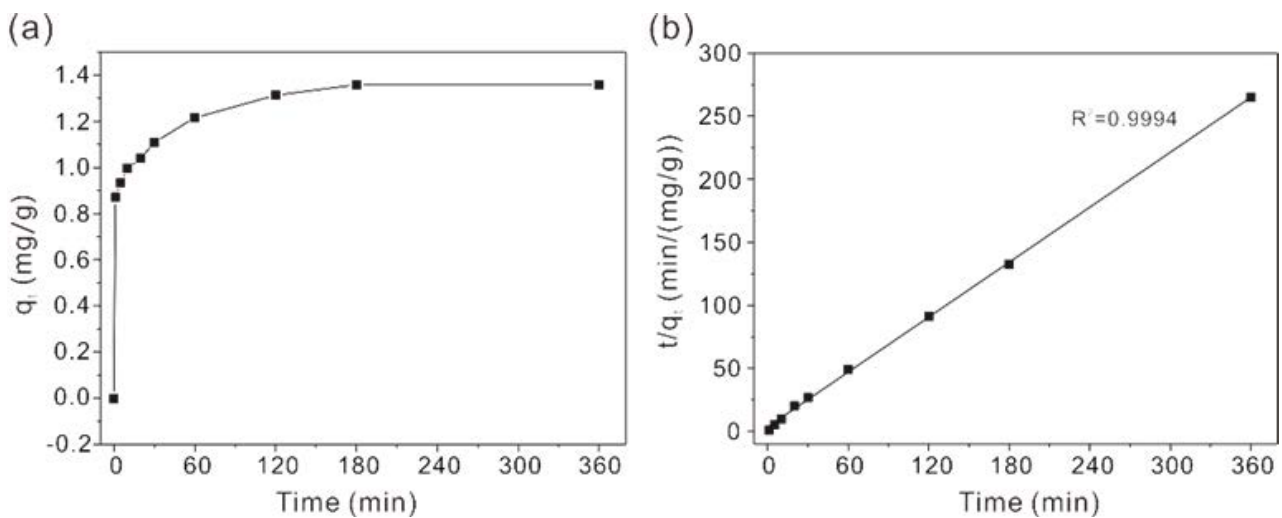

Fig. 5. Adsorption kinetics (a) and the pseudo-second-order kinetics plot (b) for fluoride adsorption on Fe_3O_4 NPs. ($C_0 = 2.5$ mg L^{-1}, temperature = 25°C, adsorbent dose = 1 g L^{-1}, pH = 7.0)

Table 1
The characteristics of kinetic models of fluoride for fitting of the experimental results

Temperature (°C)	q (mg g^{-1})	First-order			Second-order		
		k_1	R^2	q_e (mg/g)	k_2	R^2	q_e (mg/g)
25	1.312	0.0058	0.926	0.855	0.094	0.999	1.310

the pseudo-first-order model. The time required to reach adsorption equilibrium was 180 min [35].

Pseudo-first-order kinetic model:

$$\ln\left(q_e - q_t\right) = \ln q_e - k_1 t \tag{3}$$

Pseudo-second-order model:

$$\frac{t}{q_t} = \frac{1}{k_2 q_e^2} + \frac{t}{q_e} \tag{4}$$

where k_1 and k_2 are the rate constants (in g mg^{-1} min^{-1}) of the pseudo-first-order and pseudo-second-order models, q_t is the amount of fluoride adsorbed at any time (mg g^{-1}), q_e is the equilibrium adsorption capacity (mg g^{-1}).

Additionally, Bangham's equation has been used to describe pore diffusion during the adsorption process. The mathematical representation of the pore diffusion model was expressed as follows [36]:

Bangham's equation:

$$\log\log\left(\frac{C_0}{C_0 - C_s q_t}\right) = \log\left(\frac{K_b C_s}{2.303V}\right) + \alpha \log t \tag{5}$$

where C_s is the weight of adsorbent (g L^{-1}), ($\alpha < 1$) and K_b are constants calculated separately from the intercept and slope of the straight-line plots which are shown in Fig. 6. Bangham's plot was found linear with a good correlation coefficient of 0.997 indicating the adsorption kinetics was limited by the pore diffusion.
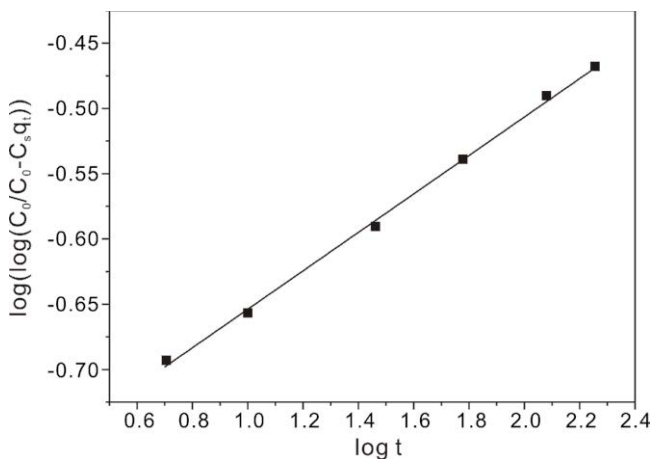

Fig. 6. Diffusion-based model for adsorption of fluoride onto Fe$_3$O$_4$ NPs.

3.2.2. Adsorption isotherm analysis

Furthermore, to understand the effect of temperature on the removal of fluoride on Fe$_3$O$_4$ NPs, the fluoride adsorption experiments were conducted at three different temperatures namely 25°C, 35°C and 45°C, and the adsorption isotherms are shown in Fig. 7. The results revealed that the adsorption properties of the Fe$_3$O$_4$ NPs declined with the increasing temperature. A good adsorption capacity of 70.64 mg g^{-1} can be achieved at 25°C. Two isotherm models of Langmuir and Freundlich were used to fit the experimental adsorption equilibrium data. These models are represented mathematically as follows [37]:

Freundlich isotherm:

$$\ln q_e = \frac{1}{n}\ln C_e + \ln K_F \tag{6}$$

Langmuir isotherm:

$$\frac{C_e}{q_e} = \frac{1}{q_m K_L} + \frac{C_e}{q_m} \tag{7}$$

where C_e (mg L^{-1}) is the concentration of fluoride at equilibrium, q_m (mg g^{-1}) is the maximum amount of fluoride adsorbed per mass of adsorbent; K_L (L mg^{-1}) is the equilibrium adsorption constant related to the affinity of binding sites; K_F (mg$^{1-(1/n)}$ L$^{1/n}$ g^{-1}) and $1/n$ are the Freundlich constants related to the adsorption capacity and intensity, respectively. It had been reported that the Freundlich model was generally adopted to describe the adsorption process on a heterogeneity surface while the Langmuir model was appropriate to simulate a monolayer adsorption process on a homogenous surface. The results of fitting Freundlich and Langmuir equations to isotherm curves are summarized in Table 2. Regression coefficients R^2 of Freundlich model for different conditions were all over 0.99, which were larger than those of Langmuir model, indicating that Freundlich model fitted reasonably better with the fluoride adsorption. Moreover, the K_F value decreased gradually with the elevation of temperature, suggesting the defluoridation process was exothermic.

For comparison, the adsorption properties of diverse adsorbents toward fluoride are listed in Table 3. Compared with many other adsorbents, like ferric hydroxide, boehmite, basic oxygen furnace slag and calcite, the Fe$_3$O$_4$ NPs in this work embraced more outstanding adsorption capacity. Though inferior to those adsorbents removing fluoride better, the Fe$_3$O$_4$ NPs had advantages in several aspects such as simple in design and synthesis, eco-friendly and low-cost.
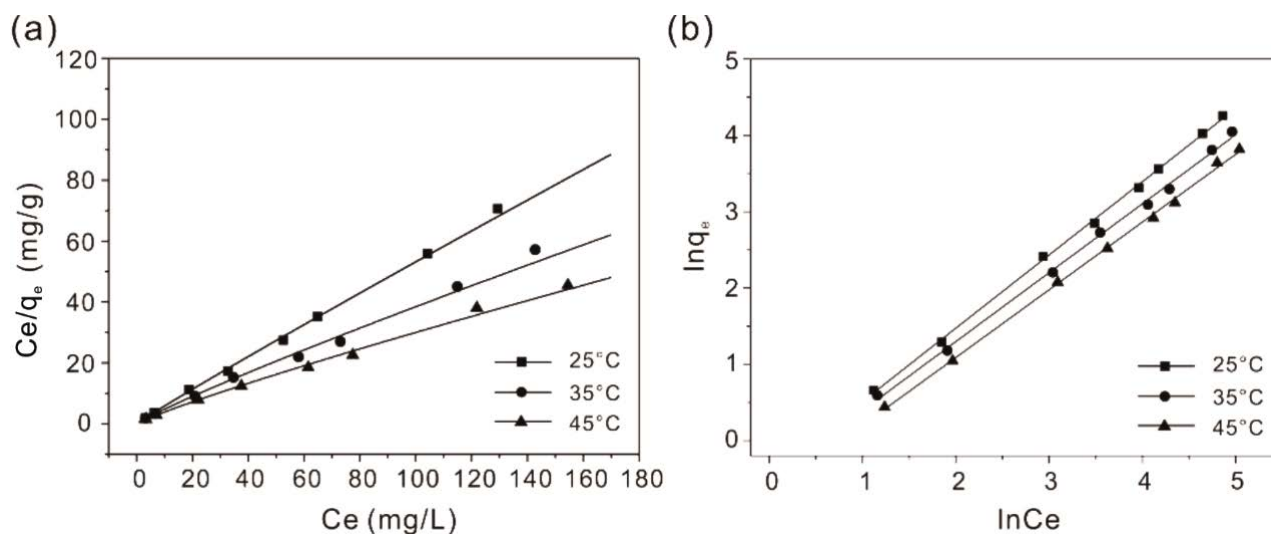
Fig. 7. Langmuir isotherms (a) and Freundlich isotherms (b) models of fluoride adsorption on Fe_3O_4 NPs (contact time = 24 h, adsorbent dose = 1 g L^{-1}, pH = 7.0).

Table 2
Langmuir and Freundlich constants for the adsorption of fluoride on Fe_3O_4 NPs at different temperatures

Temperature (°C)	Langmuir constants				Freundlich constants	
	q_m (mg g^{-1})	K_L (L mol^{-1})	R^2	$1/n$	K_F (mg g^{-1}) (L mg^{-1})$^{1/n}$	R^2
25	684.93	0.0008	0.5849	0.9597	0.6340	0.9990
35	232.56	0.0020	0.6990	0.9027	0.6018	0.9975
45	154.32	0.0025	0.7975	0.8874	0.5037	0.9986

Table 3
Comparison of the fluoride adsorption properties of various metal oxides

Adsorbents	pH	Fluoride (mg g^{-1})	Ref.
Ferric hydroxide	7	7.0	[13]
Iron(III)−tin(IV) mixed oxide	6.5	10.47	[38]
Magnetic-chitosan	7	3.0–17	[39]
PPy/Fe_3O_4	6.5	17.6−22.3	[17]
2-line ferrihydrite	7	23.89	[40]
Activated carbon	3.5	2.5	[41]
Sulfate-doped Fe_3O_4/Al_2O_3	7	70.4	[31]
Fe−Al−Ce	7.0	178	[42]
Al_2O_3/CNTs	6	28.7	[43]
Fe_3O_4 NPs	7	70.64	This work

3.2.3. Effect of the adsorbent dosage

The effect of adsorbent dosage (5−200 mg) on the removal of fluoride was investigated with two different initial fluoride concentrations namely 2.5 mg L^{-1}, 5.0 mg L^{-1}. The percent removal of fluoride was increased with the adsorbent dosage rising and reached up to its maximum at 100 mg of Fe_3O_4 NPs. No further elevation of removal rate was observed by increasing the adsorbent dose. Therefore, 0.1 g of the adsorbent was considered as the optimum dose when the initial fluoride concentration was not very high.

3.2.4. Effect of the pH value

The pH value is an important water chemistry parameter and could be significantly interfered with in the fluoride removal process. Fluoride adsorption behavior

of the Fe_3O_4 NPs was explored under different pH conditions (3~11) to assess the influence of pH to determine the pH region of maximum performance presented in Fig. 9. The removal rate was highest at pH 7, decreasing slowly in the enhanced acid condition while rapidly with the increased alkalinity. In an alkaline medium, the hydroxyl groups would compete with fluoride ions in the active sites of the adsorbent, which might be the cause for the decline of the defluoridation efficiency.

The influence of the pH on the zeta potentials of the adsorbent is shown in Fig. 10. The point of zero charges (pH_{PZC}) of the Fe_3O_4 NPs was about pH 7.38. After fluoride removal, the surface charges were decreased in the pH range of 3~11, especially in acidic conditions. When pH was lower than 7.38, the surface of adsorbents was positively charged, leading to the fluoride removed mainly through electrostatic attraction. Contrarily, as pH was h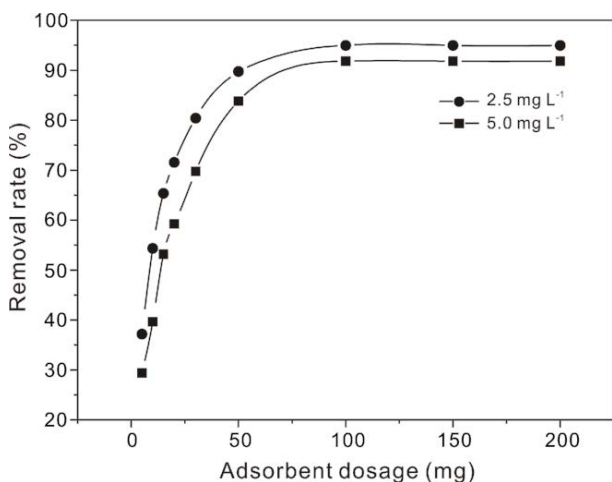igher than 7.38, the surface of adsorbents was negatively charged, tending to repel the fluoride ions via electrostatic repulsion. In this condition, the fluoride removal might be primarily based on hydroxyl exchange.

3.2.5. Effect of competing anions

Drinking water usually contains several anions like chloride, nitrate, sulfate, phosphate, bicarbonate and carbonate. Consequently, they will compete with fluoride anions for the adsorption sites. The effect of coexisting anion was evaluated at different concentrations (0~200 mg L^{-1}) and results are depicted in Fig. 11. There was no obvious change in the fluoride removal percentage when the concentration of chloride, nitrate and sulfate varied from 0 to 200 mg L^{-1}. For these three kinds of anions, the removal rates all exceeded 90%. The presence of bicarbonate, carbonate, and phosphate ions slightly reduced the fluoride adsorption that was consistent with the previously reported adsorbents.

3.3. Desorption and reusability of adsorbents

Desorption studies of spent adsorbent are essential for the economy and sustainability. In this work, NaOH was chosen as the desorption reagent for the recovery of fluoride ions from the Fe_3O_4 NPs shown in Fig. 12a. The fluoride desorption efficiencies of the adsorbent using NaOH solution of 1, 10, and 20 mM were 25.5%, 80.3%, and 95.4%, respectively, indicating that the highest recovery was obtained by using NaOH 20 mM solution. The reusability efficiency of the Fe_3O_4 NPs was investigated for five successive adsorption/desorption cycles recovered by using NaOH 20 mM solution, indicating that the adsorbent had a high regeneration efficiency (Fig. 12b). After 5 recycles, over 75% of the initial adsorption capacity was recovered, indicating the adsorbent had high reusability for the long term.

3.4. Fluoride removal mechanism

In order to clarify the fluoride removal mechanism, the mesoporous Fe_3O_4 NPs before and after fluoride

Fig. 8. Effect of the Fe_3O_4 NPs dosage on the fluoride removal (C_0 = 2.5 mg L–15.0 mg L^{-1}, temperature = 25°C, pH = 7.0).
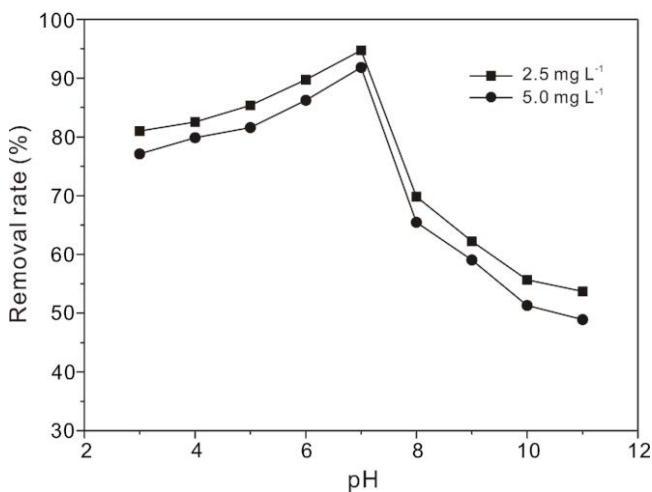

Fig. 9. The pH influence on the removal efficiency of fluoride (C_0 = 2.5–5.0 mg L^{-1}, temperature = 25°C, amount of adsorbent = 100 mg).
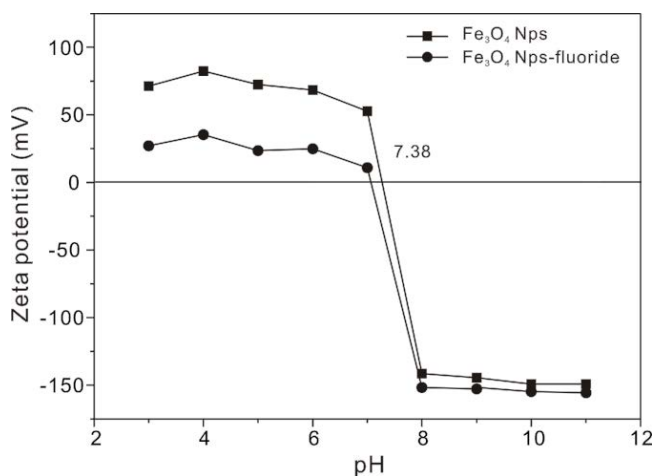

Fig. 10. Zeta potential of the Fe_3O_4 NPs in the absence and presence of fluoride as a function of pH.

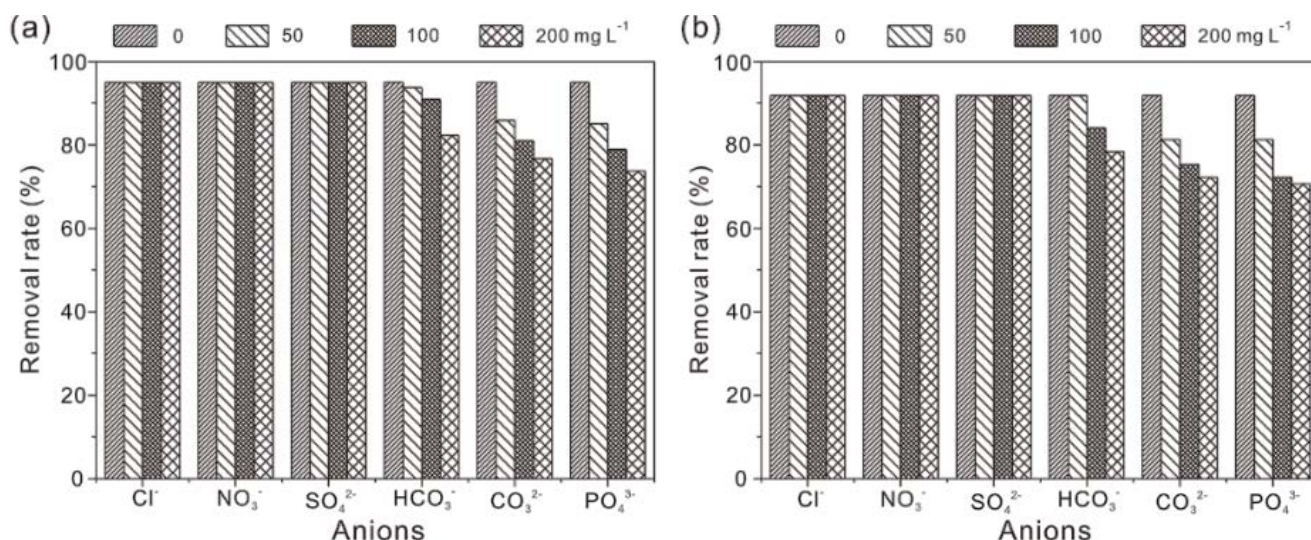Fig. 11. Effect of competing anions on fluoride adsorption (a) C_0 = 2.5 mg L^{-1} and (b) C_0 = 5.0 mg L^{-1}, temperature = 25°C, amount of and adsorbent = 100 mg).
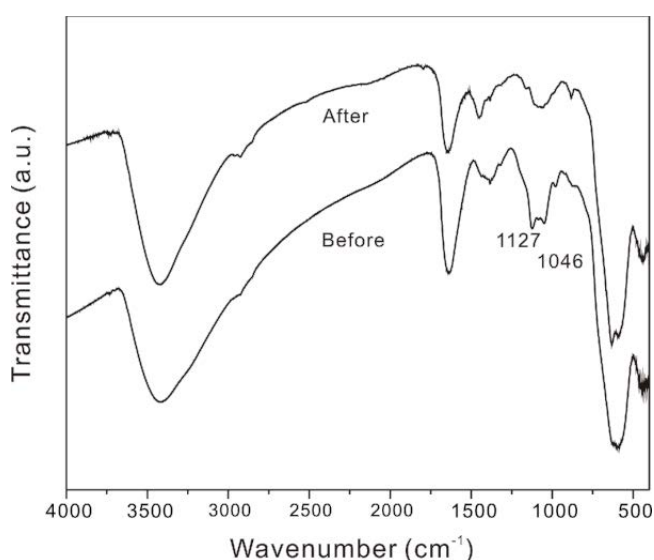

Fig. 12. FT-IR spectra of the Fe$_3$O$_4$ NPs before and after fluoride removal.

adsorption were analyzed by FT-IR shown in Fig. 13. The broad band at 3,422 cm^{-1} can be assigned to the stretching vibration of the adsorbed water, while the peak at 1,634 cm^{-1} is associated with flexural vibrations of hydroxyl groups [44]. The band observed at 1,127 cm^{-1} is attributed to the SO$_4^{2-}$ [45]. The band at 1,046 cm^{-1} belongs to hydroxo bridges bonds of the type Fe–(OH)$_2$–Fe [46]. Besides, the ν_3 vibration of SO$_4^{2-}$ can also lead to the appearance of a peak at 1,046 cm^{-1} [47]. Two peaks at 440 and 590 cm^{-1} can be attributed to Fe–O [48]. After the adsorption of fluoride, the intensity of the peak at around 1,121 and 1,046 cm^{-1} on the adsorbent significantly weaken. As surface active groups, both the sulfate and hydroxyl were reported in many literatures that they could make a great difference in the fluoride removal process. The FT–IR

results indicated that the removal mechanism was based on the ion-exchange between sulfate groups, hydroxyl groups, and fluoride anions.

The Fe$_3$O$_4$ NPs before and after fluoride removal were characterized by XPS to further clarify the fluoride removal mechanism, and the results are presented in Fig. 14. After fluoride adsorption, the fluoride characteristic peak at 684.5 eV is observed as shown in Fig. 14a, confirming the adsorption of fluoride on the adsorbent [49]. In Fig. 14b, the O1s spectrum of the virgin adsorbent can be divided into three component peaks at 529.9, 531.15, and 533.0 eV, respectively. These peaks can be assigned to metal oxide (Fe–O), hydroxyl group bonded to metal (Fe–OH) and the adsorbed water (H$_2$O) in the adsorbent [50–52], respectively. After fluoride adsorption, the relative area ratio for the peak attributed to Fe–OH decreases from 29.15% to 28.36%. Moreover, it is noted in Fig. 14c that the peak of S2p significantly decreases in the spectrum of fluoride-loaded adsorbents. In a word, its decreases indicated that sulfate and hydroxyl groups on the adsorbent surface obviously participated in the fluoride adsorption, which is in good agreement with the FT-IR results.

4. Conclusions

In summary, we presented a simple, environmentally friendly hydrothermal method to obtain Fe$_3$O$_4$ nanoparticles in a non-aqueous medium, which was confirmed by XRD, Raman spectroscopy, and XPS spectra. The adsorption properties toward fluoride were excellent with a good adsorption capacity of 70.64 mg g^{-1}. Experimental data exhibited that the fluoride removal process was well fitted with the Freundlich model and pseudo-second-order rate kinetic model. Optimization of the experimental parameters indicated a high removal rate could be reached at pH 7.0 under an adsorbent dosage of 100 mg, even in the existence of some competing anions. The study of FT-IR, XPS, and zeta potential revealed definitely that the surface
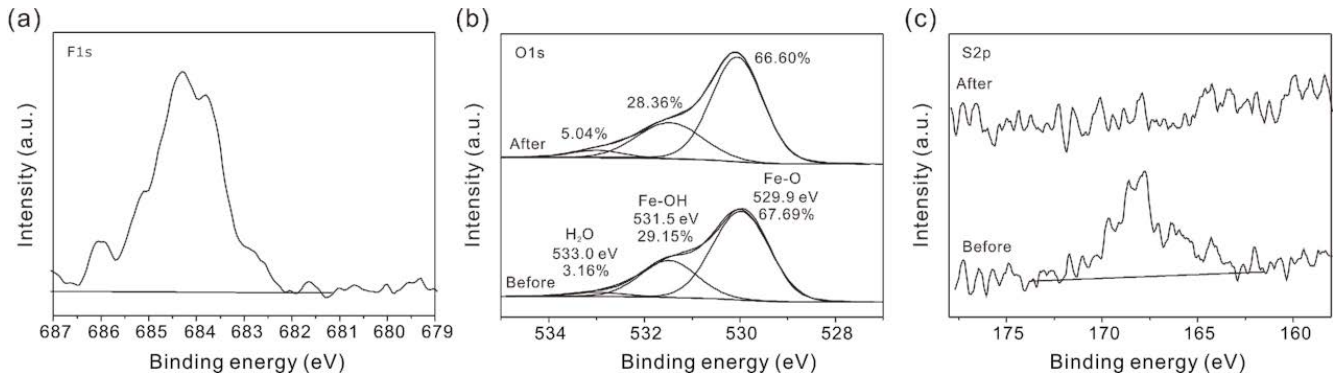
Fig. 13. XPS F1s (a) spectrum of the Fe₃O₄ NPs after fluoride removal; XPS O1s, (b) spectra of the Fe₃O₄ NPs before and after fluoride removal; XPS S2p and (c) spectra of the Fe₃O₄ NPs before and after fluoride removal.

sulfate anions and hydroxyl groups played a vital role in the removal processes of fluoride. The perfect magnetic properties, along with outstanding adsorption capacity, undoubtedly spotlighted the practical application of Fe₃O₄ nanoparticles for defluoridation.

References

[1] X.D. He, P.Y. Li, Y.J. Ji, Y.H. Wang, Z.M. Su, E. Vetrimurugan, Groundwater arsenic and fluoride and associated arsenicosis and fluorosis in China: occurrence, distribution and management, Exposure Health, 12 (2020) 355−368.
[2] T. Chernet, Y. Travi, V. Valles, Mechanism of degradation of the quality of natural water in the Lakes Region of the Ethiopian rift valley, Water Res., 35 (2001) 2819−2832.
[3] M. Mohapatra, S. Anand, B.K. Mishra, D.E. Giles, P. Singh, Review of fluoride removal from drinking water, J. Environ. Manage., 91 (2009) 67−77.
[4] L. Valdez-Jimenez, C.S. Fregozo, M.L.M. Beltran, O.G. Coronado, M.I.P. Vega, Effects of the fluoride on the central nervous system, Neurologia, 26 (2011) 297−300.
[5] S. Shahab, G. Mustafa, I. Khan, M. Zahid, M. Yasinzai, N. Ameer, N. Asghar, I. Ullah, A. Nadhman, A. Ahmed, I. Munir, A. Mujahid, T. Hussain, M.N. Ahmad, S.S. Ahmad, Effects of fluoride ion toxicity on animals, plants, and soil health: a review, Fluoride, 5 (2017) 393−408.
[6] J.Y. He, Y. Yang, Z.J. Wu, C. Xie, K.S. Zhang, L.T. Kong, J.H. Liu, Review of fluoride removal from water environment by adsorption, J. Environ. Chem. Eng., 8 (2020) 104516, doi: 10.1016/j.jece.2020.104516.
[7] L.H. Velazquez-Jimenez, R.H. Hurt, J. Matos, J.R. Rangel-Mendez, Zirconium-carbon hybrid sorbent for removal of fluoride from water: oxalic acid mediated Zr(IV) assembly

and adsorption mechanism, Environ. Sci. Technol., 48 (2014) 1166−1174.
[8] M.J. Addison, M.O. Rivett, H. Robinson, A. Fraser, A.M. Miller, P. Phiri, P. Mleta, R.M. Kalin, Fluoride occurrence in the lower East African Rift System, Southern Malawi, Sci. Total Environ., 712 (2020) 136260, doi: 10.1016/j.scitotenv.2019.136260.
[9] D.H. Phillips, B. Sen Gupta, S. Mukhopadhyay, A.K. Sen Gupta, Arsenic and fluoride removal from contaminated drinking water with Haix-Fe-Zr and Haix-Zr resin beads, J. Environ. Manage., 215 (2018) 132−142.
[10] Z.C. Yu, C.H. Xu, K.K. Yuan, X.Z. Gan, C. Feng, X.Q. Wang, L.Y. Zhu, G.H. Zhang, D. Xu, Characterization and adsorption mechanism of ZrO₂ mesoporous fibers for health-hazardous fluoride removal, J. Hazard. Mater., 346 (2018) 82−92.
[11] J.G. Cai, X. Zhao, Y.Y. Zhang, Q.X. Zhang, B.C. Pan, Enhanced fluoride removal by La-doped Li/Al layered double hydroxides, J. Colloid Interface Sci., 509 (2018) 353−359.
[12] R.M. Hegde, R.M. Rego, K.M. Potla, M.D. Kurkuri, M. Kigga, Bio-inspired materials for defluoridation of water: a review, Chemosphere, 253 (2020) 126657, doi: 10.1016/j.chemosphere.2020.126657.
[13] E. Kumar, A. Bhatnagar, M. Ji, W. Jung, S.H. Lee, S.J. Kim, G. Lee, H. Song, J.Y. Choi, J.S. Yang, B.H. Jeon, Defluoridation from aqueous solutions by granular ferric hydroxide (GFH), Water Res., 43 (2009) 490−498.
[14] M. Mohapatra, D. Hariprasad, L. Mohapatra, S. Anand, B.K. Mishra, Mg-doped nano ferrihydrite-a new adsorbent for fluoride removal from aqueous solutions, Appl. Surf. Sci., 258 (2012) 4228−4236.
[15] M. Mohapatra, T. Padhi, S. Anand, B.K. Mishra, CTAB mediated Mg-doped nano Fe₂O₃: synthesis, characterization, and fluoride adsorption behavior, Desal. Water Treat., 50 (2012) 376−386.
[16] T. Poursaberi, M. Hassanisadi, K. Torkestani, M. Zare, Development of zirconium (IV)-metalloporphyrin grafted Fe₃O₄ nanoparticles for efficient fluoride removal, Chem. Eng. J., 189 (2012) 117−125.
[17] M. Bhaumik, T.Y. Leswifi, A. Maity, V.V. Srinivasu, M.S. Onyango, Removal of fluoride from aqueous solution by polypyrrole/Fe₃O₄ magnetic nanocomposite, J. Hazard. Mater., 186 (2011) 150−159.
[18] A.R. Mandavian, M.A.S. Mirrahimi, Efficient separation of heavy metal cations by anchoring polyacrylic acid on superparamagnetic magnetite nanoparticles through surface modification, Chem. Eng. J., 159 (2010) 264−271.
[19] Y.Y. Zheng, X.B. Wang, L. Shang, C.R. Li, C. Cui, W.J. Dong, W.H. Tang, B.Y. Chen, Fabrication of shape controlled Fe₃O₄ nanostructure, Mater. Charact., 61 (2010) 489−492.
[20] D. Kim, J. Park, K. An, N.K. Yang, J.G. Park, T. Hyeon, Synthesis of hollow iron nanoframes, J. Am. Chem. Soc., 129 (2007) 5812−5813, doi: 10.1021/ja070667m.
[21] A.M.G. Domacena, C.L.E. Aquino, M.D.L. Balela, Photo-Fenton degradation of methyl orange using hematite (α-Fe₂O₃) of various morphologies, Mater. Today: Proc., 22 (2020) 248−254.

[22] N.B. Dewage, A.S. Liyanage, C.U. Pittman, D. Mohan, T. Mlsna, Fast nitrate and fluoride adsorption and magnetic separation from water on α-Fe$_2$O$_3$ and Fe$_3$O$_4$ dispersed on Douglas fir biochar, Bioresource Technol., 263 (2018) 258–265.

[23] A.A. Markeb, A. Alonso, A. Sanchez, X. Font, Adsorption process of fluoride from drinking water with magnetic core-shell Ce-Ti@Fe$_3$O$_4$ and Ce-Ti oxide nanoparticles, Sci. Total Environ., 598 (2017) 949–958.

[24] B.S. Zhu, Y. Jia, Z. Jin, B. Sun, T. Luo, X.Y. Yu, L.T. Kong, X.J. Huang, J.H. Liu, Controlled synthesis of natroalunite microtubes and spheres with excellent fluoride removal performance, Chem. Eng. J., 271 (2015) 240–251.

[25] K. Biswas, K. Gupta, A. Goswami, U.C. Ghosh, Fluoride removal efficiency from aqueous solution by synthetic iron(III)-aluminum(III)-chromium(III) ternary mixed oxide, Desalination, 255 (2010) 44–51.

[26] W. Ma, T.F. Lv, X.Y. Song, Z.H. Cheng, S.B. Duan, G. Xin, F.J. Liu, D.C. Pan, Characteristics of selective fluoride adsorption by biocarbon-Mg/Al layered double hydroxides composites from protein solutions: kinetics and equilibrium isotherms study, J. Hazard. Mater., 268 (2014) 166–176.

[27] K.S.K. Varadwaj, M.K. Panigrahi, J. Ghose, Effect of capping and particle size on Raman laser-induced degradation of gamma-Fe$_2$O$_3$ nanoparticles, J. Solid State Chem., 177 (2004) 4286–4292.

[28] X.B. Hu, M.H. Ma, M.Q. Zeng, Y.Y. Sun, L.F. Chen, Y.H. Xue, T. Zhang, X.P. Ai, R.G. Mendes, M.H. Rummeli, L. Fu, Supercritical carbon dioxide anchored Fe$_3$O$_4$ nanoparticles on graphene foam and lithium battery performance, ACS Appl. Mater. Interfaces, 6 (2014) 22527–22533.

[29] C. Gao, X.Y. Yu, S.Q. Xiong, J.H. Liu, X.J. Huang, Electrochemical detection of Arsenic(III) completely free from noble metal: Fe$_3$O$_4$ microspheres-room temperature ionic liquid composite showing better performance than gold, Anal Chem., 85 (2013) 2673–2680.

[30] J. Wang, W.H. Xu, L. Chen, Y. Jia, L. Wang, X.J. Huang, J.H. Liu, Excellent fluoride removal performance by CeO$_2$-ZrO$_2$ nanocages in water environment, Chem. Eng. J., 231 (2013) 198–205.

[31] L.Y. Chai, Y.Y. Wang, N. Zhao, W.C. Yang, X.Y. You, Sulfate-doped Fe$_3$O$_4$/Al$_2$O$_3$ nanoparticles as a novel adsorbent for fluoride removal from drinking water, Water Res., 47 (2013) 4040–4049.

[32] F. Rojas, I. Kornhauser, C. Felipe, J.M. Esparza, S. Cordero, A. Dominguez, J.L. Riccardo, Capillary condensation in heterogeneous mesoporous networks consisting of variable connectivity and pore-size correlation, Phys. Chem. Chem. Phys., 4 (2002) 2346–2355.

[33] L.Y. Feng, M.H. Cao, X.Y. Ma, Y.S. Zhu, C.W. Hu, Superparamagnetic high-surface-area Fe$_3$O$_4$ nanoparticles as adsorbents for arsenic removal, J. Hazard. Mater., 217 (2012) 439–446.

[34] T. Luo, Q.Q. Meng, C. Gao, X.Y. Yu, Y. Jia, B. Sun, Z. Jin, Q.X. Li, J.H. Liu, X.J. Huang, Sub-20 nm-Fe$_3$O$_4$ square and circular nanoplates: synthesis and facet-dependent magnetic and electrochemical properties, Chem. Commun., 50 (2014) 15952–15955.

[35] W. Ma, N.N. Zhao, G. Yang, L.Y. Tian, R. Wang, Removal of fluoride ions from aqueous solution by the calcination product of Mg-Al-Fe hydrotalcite-like compound, Desalination, 268 (2011) 20–26.

[36] Y. Jia, B.S. Zhu, K.S. Zhang, Z. Jin, B. Sun, T. Luo, X.Y. Yu, L.T. Kong, J.H. Liu, Porous 2-line ferrihydrite/bayerite composites (LFBC): fluoride removal performance and mechanism, Chem. Eng. J., 268 (2015) 325–336.

[37] W.X. Gong, J.H. Qu, R.P. Liu, H.C. Lan, Adsorption of fluoride onto different types of aluminas, Chem. Eng. J., 189 (2012) 126–133.

[38] K. Biswas, K. Gupta, U.C. Ghosh, Adsorption of fluoride by hydrous iron(III)-tin(IV) bimetal mixed oxide from the aqueous solutions, Chem. Eng. J., 149 (2009) 196–206.

[39] W. Ma, F.Q. Ya, M. Han, R. Wang, Characteristics of equilibrium, kinetics studies for adsorption of fluoride on magnetic-chitosan particle, J. Hazard. Mater., 143 (2007) 296–302.

[40] B.S. Zhu, Y. Jia, Z. Jin, B. Sun, T. Luo, L.T. Kong, J.H. Liu, A facile precipitation synthesis of mesoporous 2-line ferrihydrite with good fluoride removal properties, RSC Adv., 5 (2015) 84389–84397.

[41] R.L. Ramos, J. Ovalle-Turrubiartes, M.A. Sanchez-Castillo, Adsorption of fluoride from aqueous solution on aluminum-impregnated carbon, Carbon, 37 (1999) 609–617.

[42] X. Wu, Y. Zhang, X. Dou, M. Yang, Fluoride removal performance of a novel Fe-Al-Ce trimetal oxide adsorbent, Chemosphere, 69 (2007) 1758–1764.

[43] Y.H. Li, S.G. Wang, A.Y. Cao, D. Zhao, X.F. Zhang, C.L. Xu, Z.K. Luan, D.B. Ruan, J. Liang, D.H. Wu, B.Q. Wei, Adsorption of fluoride from water by amorphous alumina supported on carbon nanotubes, Chem. Phys. Lett., 350 (2001) 412–416.

[44] Y. Zhang, M. Yang, X.M. Dou, H. He, D.S. Wang, Arsenate adsorption on an Fe-Ce bimetal oxide adsorbent: role of surface properties, Environ. Sci. Technol., 39 (2005) 7246–7253.

[45] A. Halajnia, S. Oustan, N. Najafi, A.R. Khataee, A. Lakzian, Adsorption-desorption characteristics of nitrate, phosphate and sulfate on Mg-Al layered double hydroxide, Appl. Clay Sci., 80–81 (2013) 305–312.

[46] N. Papassiopi, K. Vaxevanidou, C. Christou, E. Karagianni, G.S.E. Antipas, Synthesis, characterization and stability of Cr(III) and Fe(III) hydroxides, J. Hazard. Mater., 264 (2014) 490–497.

[47] H. Wijnja, C.P. Schulthess, Vibrational spectroscopy study of selenate and sulfate adsorption mechanisms on Fe and Al (hydr)oxide surfaces, J. Colloid. Interf. Sci., 229 (2000) 286–297.

[48] Z. Li, L. Wei, M.Y. Gao, H. Lei, One-pot reaction to synthesize biocompatible magnetite nanoparticles, Adv. Mater., 17 (2005) 1001–1005.

[49] L. Chen, K.S. Zhang, J.Y. He, W.H. Xu, X.J. Huang, J.H. Liu, Enhanced fluoride removal from water by sulfate-doped hydroxyapatite hierarchical hollow microspheres, Chem. Eng. J., 285 (2016) 616–624.

[50] S.B. Deng, H. Liu, W. Zhou, J. Huang, G. Yu, Mn-Ce oxide as a high-capacity adsorbent for fluoride removal from water, J. Hazard. Mater., 186 (2011) 1360–1366.

[51] Y. Yu, L. Yu, J.P. Chen, Adsorption of fluoride by Fe-Mg-La triple-metal composite: adsorbent preparation, illustration of performance and study of mechanisms, Chem. Eng. J., 262 (2015) 839–846.

[52] A.P. Grosvenor, B.A. Kobe, N.S. McIntyre, Studies of the oxidation of iron by water vapour using X-ray photoelectron spectroscopy and QUASES (TM), Surf. Sci., 572 (2004) 217–227.

Supporting information

Fig. S1. Photographs of Fe$_3$O$_4$ nanocomposites.